Published in final edited form as:
Cell. 2014 May 8; 157(4): 808–822. doi:10.1016/j.cell.2014.02.056.

Structurally Distinct Ca^{2+} Signaling Domains of Sperm Flagella Orchestrate Tyrosine Phosphorylation and Motility

Jean-Ju Chung[1,2,6], **Sang-Hee Shim**[4,6,7], **Robert A. Everley**[3], **Steven P. Gygi**[3], **Xiaowei Zhuang**[4,5,*], and **David E. Clapham**[1,2,*]

[1]Howard Hughes Medical Institute, Department of Cardiology, Boston Children's Hospital, 320 Longwood avenue, Boston, MA 02115, USA

[2]Department of Neurobiology, Harvard Medical School, 220 Longwood avenue, Boston, MA 02115, USA

[3]Department of Cell Biology, Harvard Medical School, 240 Longwood avenue, Boston, MA 02115, USA

[4]Howard Hughes Medical Institute, Department of Chemistry and Chemical Biology, Cambridge, MA, 02138, USA

[5]Department of Physics, Harvard University, 12 Oxford street, Cambridge, MA 02138, USA

SUMMARY

Spermatozoa must leave one organism, navigate long distances, and deliver their paternal DNA into a mature egg. For successful navigation and delivery, a sperm-specific calcium channel is activated in the mammalian flagellum. The genes encoding this channel (*CatSpers*) appear first in ancient uniflagellates, suggesting that sperm use adaptive strategies developed long ago for single cell navigation. Here, using genetics, super-resolution fluorescence microscopy, and phosphoproteomics, we investigate the CatSper-dependent mechanisms underlying this flagellar switch. We find that the CatSper channel is required for four linear calcium domains that organize signaling proteins along the flagella. This unique structure focuses tyrosine phosphorylation in time and space as sperm acquire the capacity to fertilize. In heterogeneous sperm populations, we find unique molecular phenotypes, but only sperm with intact CatSper domains that organize time-dependent and spatially specific protein tyrosine phosphorylation successfully migrate. These findings illuminate flagellar adaptation, signal transduction cascade organization, and fertility.

Freshly ejaculated mammalian spermatozoa are unable to fertilize. In the female reproductive tract, sperm undergo changes that enable them to fertilize in a process called

*Correspondence: dclapham@enders.tch.harvard.edu (D.E.C), zhuang@chemistry.harvard.edu (X.Z.).
[6]These authors contributed equally to this work
[7]Present address: Department of Biomedical Engineering, School of Life Sciences, Ulsan National Institute of Science and Technology, UNIST-gil 50, Ulsan 689–798, Republic of Korea

capacitation (Chang, 1951). Well-established cellular changes during capacitation include an increase in intracellular calcium and abundant tyrosine phosphorylation of flagellar proteins (Baldi et al., 1991; Visconti et al., 1995a). Calcium signaling specificity is accomplished via the ion's spatiotemporal localization. Precise subcellular localization and scaffolding of Ca^{2+} channel complexes with signaling cascades is essential in specialized cells (Clapham, 2007). Mammalian sperm, a highly specialized cell, has elaborate cytoskeletal structures in the tail for motility regulation. Hyperactivated motility, a powerful, asymmetric, whip-like motion of the tail is the physical manifestation of capacitation (Yanagimachi, 1994). Hyperactivation requires CatSper, a flagellar specific and Ca^{2+}-selective channel encoded by at least 7 genes (*CatSpers1–4*, β, γ, and δ). Male mice lacking any of the *CatSper1–4*, or δ genes are infertile (Chung et al., 2011; Qi et al., 2007; Quill et al., 2003; Ren et al., 2001), as are human males with loss-of-function mutations (Avenarius et al., 2009; Avidan et al., 2003; Smith et al., 2013). A prominent marker of mammalian capacitation is extensive tyrosine phosphorylation (P-Tyr) of sperm proteins, which in turn is positively regulated by cAMP-dependent kinase (PKA) (Visconti et al., 1995b). Bicarbonate activates sperm soluble adenylyl cyclase (SACY) that increases cAMP and PKA activity (Chen et al., 2000), and raises intracellular pH to activate CatSper channels (Kirichok et al., 2006). Yet there are major unresolved links between these events and motility changes during capacitation.

The sperm axoneme is a 9+2 structure comprised of a central pair of singlet microtubules surrounded by 9 doublet microtubules. Dynein ATPases linking doublet microtubules drive their relative motion, but in mammalian sperm, the overall planar stroke, bend, and rotation of the flagella may be modulated by outer dense fibers (ODFs) and the fibrous sheath (FS) that separate the axoneme from the plasma membrane (Eddy et al., 2003; Fawcett, 1975). Submicron flagellar dimensions have hidden much of the relevant cell biology from visualization. Although the cytoskeletal structures of sperm flagella can be studied by electron microscopy (EM) (Fawcett, 1970), ultrastructural visualization of specific proteins is complicated by low labeling efficiency.

Here we use super-resolution fluorescence microscopy (Heintzmann and Gustafsson, 2009; Hell, 2009; Huang et al., 2010; Patterson et al., 2010) to determine the three-dimensional distributions of proteins within single flagella at nanometer-scale resolution. We find that the CatSper channel forms a quadrilateral arrangement in 3 dimensions that organizes structurally distinct Ca^{2+} signaling domains ('Ca^{2+} domains') along the flagella. We use genetic deletions to show that CatSper is essential in organizing Ca^{2+} signaling molecules such as CaMKII, calcineurin (PP2B-Aγ), and caveolin-1 into these domains. Surprisingly, protein tyrosine phosphorylation (P-Tyr) delocalizes upon disruption of the CatSper channel, indicating a functional connection between the two major signaling pathways in sperm capacitation. Using a phosphoproteomic approach, we profiled P-Tyr sites common to both *WT* and *CatSper1-null* spermatozoa and find that Src family kinases (SFK) are involved in the spatial control of P-Tyr. During capacitation, CatSper1 and the signaling molecules in these domains all undergo dramatic changes, which generate heterogeneous sperm populations. Finally, we demonstrate that intact Ca^{2+} domains are indispensible for hyperactivated motility, which we correlate with normal sperm migration *in vivo*.

RESULTS

Sperm Ultrastructure in 3-D by STORM

To determine the spatial organization of CatSper and downstream intraflagellar signaling, we used stochastic optical reconstruction microscopy (STORM). STORM enables volumetric reconstruction at ~20-nm lateral and ~50-nm axial resolutions (Huang et al., 2008b; Rust et al., 2006). Since the sperm tail is usually less than 1-εm wide, we visualized the molecular distribution across an entire flagellum with 3D STORM. As initial controls, we determined the spatial distributions of well-studied sperm flagellar proteins, labeled with specific antibodies and dye-conjugated secondary antibodies (Figure 1B–E, G; Figure S1A–D) and compared these to transmission electron micrographs (TEM) (Figure 1A, F; Figure S1E). Glucose transporter 3 (GLUT3), a member of the facilitative glucose transporter family, is present throughout the flagellar plasma membrane (Simpson et al., 2008) (Figure S1A). As expected, 3D STORM images of GLUT3 show a continuous surface rim in cross-section and a uniform distribution along the flagella (Figure 1B). STORM images of the sperm structural proteins, such as fibrous sheath-localized A kinase anchoring protein 4 (AKAP4), outer dense fiber protein 2 (ODF2), and axonemal α/β-tubulin, correspond to the distribution and localization found in TEM images (Fawcett, 1970; Johnson et al., 1997; Schalles et al., 1998) (Figure 1C–G; Figure S1E), validating the ultrastructural information obtained by 3D STORM.

CatSper in 4 Linear Domains along the Flagellum

We next investigated the distribution of CatSper channels on the flagella. CatSper channel staining is highest in the first half of principal piece (Chung et al., 2011; Liu et al., 2007; Ren et al., 2001) (Figure 2A; Figure S2A–C). In contrast to the even surface distribution of GLUT3, CatSper1 proteins form a unique pattern of four linear ‘stripes’ running down the principal piece of the flagellum (Figure 2B; Movie S1). On cross-sections of the flagellum, they appear as 4 tight clusters (Figure 2C; Figure S2D) and are represented as 4 lines in the 2D angular profiles of the surface localizations (Figure S2E, F). CatSperδ, one of the 5 subunits known to be required for functional channel formation (Chung et al., 2011), co-localizes precisely with CatSper1 in this quadrilateral structure (Figure 2D–F; Figure S2G, H). CatSperβ, another CatSper accessory subunit, has an identical distribution (*data not shown*). Since all 7 CatSper subunits form a protein complex and 5 of these are proven to be required for function (Chung et al., 2011; Kirichok et al., 2006; Qi et al., 2007), we presume that all CatSper subunits colocalize within these linear domains.

CatSper1 antibodies were suitable for immuno-EM and confirmed the quadrilateral localization of CatSper1 (Figure 2G, H). In EM, the 4-fold CatSper structure is apparent as two double rows, each row on either side of the longitudinal columns (Figure 2I–K). These micrographs reveal precise positional information with respect to underlying cytoskeletal structures. How does this striking degree of 3-D organization serve the sperm’s unique functions?

CatSper Colocalizes with Ca^{2+} Signaling Molecules

The compartmentalization of the CatSper channel complex within flagellar membrane suggests that, analogous to functional Ca^{2+} compartments found in neuronal, immunological synapses and cilia, these structures create functional domains of Ca^{2+} signaling molecules. Indeed, we found a CatSper-like distribution for the constitutively active form of CaMKII (phosphorylated at threonine 286, P-CaMKII; Figure 3A) in the principal piece. Similar to CaMKII, the testis-specific catalytic subunit of calcineurin (Protein phosphatase 2B; PP2B-Aγ) (Muramatsu et al., 1992; Tash et al., 1988) is in the principal piece (Figure S3A, A') and localized to the quadrilateral structures (Figure 3B). PP2B-Aγ also localizes to the axonemal region of the principal piece (Figure 3B), in agreement with calcineurin's firm binding to dynein (Muramatsu et al., 1992).

Like P-CaMKII (T286), PP2B-Aγ and CatSper, caveolin-1 is localized to the principal piece (Travis et al., 2001) (Figure S3B, C) and co-localizes in quadrilateral domains (Figure 3C, *right*; Figure S3D–F). In contrast, another principal piece-specific protein, plasma membrane Ca^{2+} ATPase 4 (PMCA4; a Ca^{2+} extrusion pump), is membrane associated but not with any distinct organization (Figure S3G, I, K). The ubiquitous, soluble, and abundant Ca^{2+} adaptor protein, calmodulin, appears to fill the entire flagella except for the fibrous sheath region (Figure S3H, H', J). These results suggest that the CatSper-defined quadrilateral structure is a Ca^{2+} signaling domain including CaMKII (P-T286), PP2B-Aγ, and caveolin-1.

CatSper, not Caveolin-1, is Essential in Organizing Ca^{2+} Domains

Caveolin-1 is a scaffolding protein in cholesterol-rich microdomains (Razani et al., 2002). One of the unusual changes during sperm capacitation is the exodus of cholesterol from the plasma membrane (Lin and Kan, 1996). However, caveolin-1 does not scaffold CatSper; CatSper in *caveolin-1-null* spermatozoa are localized normally (Figure S4A). Furthermore, *caveolin-1-null* mice are fertile (Razani et al., 2001) and their sperm develop normal hyperactivated motility. In contrast to *caveolin-1-null* sperm, the *CatSper1-null* sperm Ca^{2+} domain is disrupted and proteins are mislocalized. In these mice, caveolin-1 proteins are upregulated (Figure S3C, C'), delocalize from the quadrilateral structure, and become uniformly distributed in the plasma membrane (Figure 3C', D, E; Figure S4B).

Like caveolin-1, CaMKII (P-T286) and PP2B-Aγ also delocalize in *CatSper1-null* spermatozoa (Figure 3A', B'), with CaMKII (P-T286) distributed more randomly near the membrane (Figure 3A', C', E). Interestingly, PP2B-Aγ disappears from the quadrilateral structure but remains localized primarily to the axoneme (Figure 3B', F), suggesting that there are two different pools of PP2B-Aγ in the flagella. In contrast, the spatial distributions of CaM and PMCA4 are not significantly affected (*data not shown*). Moreover, disruption of the sperm-specific K^+ channel (Slo3) and sodium hydrogen exchanger (sNHE) did not perturb the unique alignment of the CatSper Ca^{2+} domains (Figure S4C, D). Indeed, CatSper current was unchanged in both *Slo3* and *sNHE* null spermatozoa (Qi et al., 2007; Zeng et al., 2013). Thus, the CatSper channel complex may organize the Ca^{2+} domains; in mice lacking CatSper, the entire CatSper complex fails to form and P-CaMKII, calcineurin, and caveolin-1 delocalize.

CatSper's Spatiotemporal Control of Protein Tyrosine Phosphorylation

Upon hyperactivation, the CatSper-mediated Ca^{2+} signal is translated into mechanical changes in the axoneme and may increase flagellar glycolytic production of ATP (Ho et al., 2002; Williams and Ford, 2001; Xia et al., 2007); these changes are requisite for higher force generation and larger tail bend angles. A hallmark of capacitation is abundant flagellar protein tyrosine phosphorylation (P-Tyr) (Visconti et al., 1995a; Visconti et al., 1995b), requiring glycolytically generated ATP (Urner et al., 2001). We thus investigated whether CatSper-mediated Ca^{2+} signaling and P-Tyr are linked. P-Tyr is readily detected in *WT* flagella after capacitation (Figure 4A, B). Surprisingly, we find that P-Tyr is further enhanced upon capacitation of *CatSper1-null* spermatozoa (Figure 4A (*right*), B). P-Tyr is similarly potentiated in *CatSper3-*, *4-*, and δ *-null* spermatozoa after *in vitro* capacitation (Figure S5A, B and *data not shown*). These data suggest that disruption of the CatSper channel complex deregulates the capacitation-initiated tyrosine phosphorylation pathway.

We next examined whether P-Tyr inhibition requires external Ca^{2+}. When extracellular Ca^{2+} was simply lowered with BAPTA, a Ca^{2+} chelator, or replaced with 2 mM Mg^{2+} under capacitating conditions, P-Tyr increased in *WT* spermatozoa (Figure S5C, *left*). Conversely, P-Tyr decreased when the Ca^{2+} ionophore, ionomycin or A23187 increased intracellular [Ca^{2+}] in *CatSper1-null* spermatozoa (Figure S5C, *right*). Under these conditions, however, the sperm were less motile than *WT* spermatozoa (*data not shown*). Presumably, although intraflagellar [Ca^{2+}] increases, Ca^{2+} signaling effectiveness is degraded by the loss of domain organization. We conclude that manipulating Ca^{2+} influx recapitulates the extent of P-Tyr, but proper sperm motility requires a spatially localized network.

Interestingly, the P-Tyr signal in the proximal region of the principal piece in capacitated *WT* spermatozoa is confined to a region substantially narrower than the flagellar diameter (Figure 4C, D; Figure S5D, E), roughly defined by the outer doublets of the axoneme (compare Figure 4E–F with Figure 1E–G) encompassing the radial spoke proteins. In striking contrast, P-Tyr in *CatSper1-null* sperm fills the extra-axonemal space (Figure 4E–F). Since the intensity of protein bands in immunoblots is increased in *CatSper1-null* spermatozoa (Figure 4B; Figure S5B), we examined tyrosine phosphorylation time courses. P-Tyr spreads from the center of the axoneme in *CatSper1-null* spermatozoa, but P-Tyr was initiated much earlier than in *WT* spermatozoa (Figure 4G–H; Figure S5F–H). These data indicate that the CatSper complex functionally confines P-Tyr to the axoneme. One simple hypothesis is that CatSper-mediated Ca^{2+} signaling slows P-Tyr in the peri-axonemal regions. P-Tyr is less confined to the axoneme in the distal principal piece where CatSper declines (*data not shown*).

Profiling Capacitation-associated P-Tyr Sites

Capacitation-associated P-Tyr in *WT*, and its rampant counterpart in *CatSper1-null* spermatozoa, was analyzed with affinity purification by tandem mass tagging (Ballif et al., 2008; Dephoure et al., 2013). 62 distinct P-Tyr sites on 45 proteins were detected from these two cell populations (Table 1; Table S1). In experiments run in triplicate, almost all of the 62 P-Tyr peptides were detected in both *WT* and *CatSper1-null* spermatozoa (Table S1). Of these, phosphorylation was elevated ≥ 2-fold at 41 P-Tyr sites in *CatSper1-null*

spermatozoa, comprising 66% of all P-Tyr sites identified. The remaining 21 P-Tyr KO/WT ratios varied between 0.6 and 2.0. Constitutive P-Tyr in uncapacitated spermatozoa in *WT* and *null* mice is minimal and primarily in the head (Figure 4A, B). These data suggest that P-Tyr is induced in the same pool of flagellar proteins in *WT* and *CatSper1-null* sperm, albeit to different levels during capacitation.

Table 1 is the tyrosine phosphoproteome of capacitated mouse sperm. To distinguish changes in phosphorylation from those in protein levels, phosphorylation changes were normalized to protein abundance (Table S1). Only 7 of the 62 sites, including calmodulin and hexokinase 1, were previously reported (based on comparison with the PhosphoSite database of known phosphorylation sites (Hornbeck et al., 2004)). We classified the 45 P-Tyr proteins by Gene Ontology (GO), NCBI BLASTp along with their conserved domains, and the literature (Table 1; Figure 5A). Multiple kinase signaling pathways involving separate kinase classes were identified, including the regulatory subunit α of cAMP-dependent protein kinase type II (PKA-RIIa), the dual specificity tyrosine-phosphorylation-regulated kinase 1A (DYRK1A), and the Fps/Fes related tyrosine kinase (FER). While providing an overview of tyrosine phosphorylation during capacitation, our focus is CatSper-dependent changes: in 11 out of 12 structural proteins including 5 axonemal proteins the P-Tyr ratio increased by ≥ 2-fold. These data suggest that CatSper-dependent Ca^{2+} entry is linked to P-Tyr signaling in motility regulation.

Src Family Kinases (SFK) Target CatSper-dependent Pathways

Fer is a non-receptor tyrosine kinase with a testicular isoform associated with the acrosome-acroplaxoneme-manchette complex (Kierszenbaum et al., 2008). However, *Fer-null* mice are fertile (Craig et al., 2001) and the P-Tyr site is not significantly changed between WT and *CatSper1-null* mice (Table 1). Since amino and carboxyl terminal residues to the P-Tyr site direct the specificity of tyrosine kinases, we compiled an amino acid frequency plot of center-oriented P-Tyr motif peptide sequences (Figure 5B) (Crooks et al., 2004). The C-terminal residue (P + 1) is considered most important for specific binding by prototypic SH2 domains. When the 41 CatSper-dependent sites were sorted by this position, we identified 3 motifs (y[DE], y[AG], and y[ST]) from 28 sites on 23 proteins (Figure 5C; Table S2) that fit to previously reported SFK (Src family kinase) consensus sites (Amanchy et al., 2007; Schwartz and Gygi, 2005). These comprise 68% of all the CatSper-dependent P-Tyr sites identified, suggesting that a SFK could target CatSper-dependent pathways. We examined known SFKs and their phosphorylation states in spermatozoa. Src phosphorylation at an activating site (Y416), and Lyn and Lck at inactivating sites (Y507 and Y505), increased in capacitated *CatSper1-null* spermatozoa (Figure 5D), reflecting dynamic SFK regulation (Figure 4; Figure S5). By STORM, phosphorylated Src (Y416) and Lck (Y505) were further assessed; regardless of whether the sites were activating or inactivating, the localization of tyrosine phosphorylated Src and Lck followed typical P-Tyr distributions of *WT* and *CatSper1-null* spermatozoa (Figure 5E vs. Figure 4E). Since *c-Src*-null spermatozoa develop normal P-Tyr (Krapf et al., 2010), these data suggest that the identified SFKs are redundant in the effusive tyrosine phosphorylation of *CatSper1-null* sperm.

cAMP/PKA Regulation in the Peri-axoneme

Calcium and bicarbonate activate soluble adenylyl cyclase (sAC), which catalyzes the conversion of ATP to cAMP (Chen et al., 2000; Jaiswal and Conti, 2003). Since CatSper increases flagellar [Ca^{2+}], [cAMP] and potentially PKA activity increase. H89, an inhibitor of PKA, blocked P-Tyr development in both *WT* and *CatSper1-null* spermatozoa (Figure S6A), suggesting that sAC and PKA initiate the P-Tyr cascade. However, PKA activation was more robust in *CatSper1-null* spermatozoa (Figure S6B), suggesting that regulation is more complex than direct Ca^{2+} regulation of PKA. Upon cAMP binding, regulatory subunits (RII) release catalytic subunits of PKA (PKA C) from the inactive holoenzyme, thereby increasing PKA activity. We find that PKA-RIIa is more tyrosine phosphorylated on Y382 in *CatSper1-null* spermatozoa (Table 1). This indicates that PKA-RIIa, and thus PKA activity, is modulated by a tyrosine kinase/phosphatase, a previously unrecognized molecular mechanism. Phosphorylation is enhanced at the inactivating sites of Protein Phosphatase 1 (PP1 T320) and PP2A-C (Y307) in *CatSper1-null* spermatozoa (Figure S6D). However, calyculin A, a PP1A and PP2A inhibitor, decreased P-Tyr only marginally (Figure S6A), suggesting that the SFKs could indirectly regulate PKA activity through Ser/Thr phosphatases such as PP2A or PP1.

These data and the previous literature confirm a welter of kinase/phosphatase activity during capacitation. The *CatSper* null data provide a glimpse into the kinase cascades that are primarily controlled by CatSper-driven Ca^{2+} entry, with the surprising result that SFKs appear to be spatially restricted to phosphorylating axonemal proteins when CatSper is present (Figure S6E).

Ca^{2+} Signal Transduction Focuses CaM Tyrosine Phosphorylation at the Axoneme

In the absence of CatSper, P-Tyr is increased in 5 of 9 signaling pathway proteins (Table 1). Calmodulin at Y100 ranked highest (Table S1). As a universal Ca^{2+} adaptor, calmodulin modulates many proteins; in particular, phosphorylation of CaM at this site enhances activation of PDE, PMCA, CaMKII, PP2B, and NOS (Corti et al., 1999). We assessed the expression and subcellular localization of P-CaM (Y100) using a phosphospecific Y100 CaM antibody and verified that it is potentiated in capacitated *CatSper1-null* spermatozoa (Figure 5F; protein expression of total CaM was not changed, Figure S7A, B). By STORM imaging, CaM is more concentrated in the center of the flagella with some tethered at the periphery of the flagella (Figure S3I). This distribution was not significantly changed by CatSper disruption (*data not shown*). Y100 was primarily phosphorylated in peripherally localized CaM in *CatSper-null* flagella (Figure 5G). In contrast, only the axoneme-associated fraction of CaM was tyrosine phosphorylated in *WT* spermatozoa (Figure 5G). Thus, tyrosine phosphorylation of CaM is spatially determined. CaM Y100 is not an SFK substrate (Table S2), as supported by the observed P-Tyr SFK localization in the axoneme of both *WT* and *CatSper1-null* spermatozoa (Figure 5E).

Capacitation Generates Heterogeneous Sperm Populations

We next examined the fate of CatSper Ca^{2+} domain proteins after capacitation. While the total amount of CaMKII remains unchanged, roughly half of P-CaMKII is dephosphorylated at T286 in *WT* spermatozoa after 90 min capacitation (Figure 6A, B; Figure S7A, B),

consistent with a switch from autonomous CaMKII (P-T286) activity to Ca^{2+}-dependent activity (Hudmon and Schulman, 2002). Interestingly, a higher molecular weight P-T286 CaMKII appears in *CatSper1-null* spermatozoa, perhaps due to phosphorylation at an additional site or detection of a different CaMKII isoform phosphorylated at T286. PP2B-Aγ levels also dramatically decrease. Moreover, CatSper1 protein levels decline significantly among CatSper subunits, suggesting that CatSper1 is processed (Figure 6A, B; Figure S7C, D, E - *upper*). Block of CatSper1 degradation by addition of the proteasome inhibitor, MG-132 (Figure S7E, *upper*) and specific proteolysis of recombinant CatSper1 by sperm lysates *in vitro* (Figure S7E, *lower*) suggest that proteolytic enzymes in sperm process CatSper1.

Protein levels changes are population averages, but capacitation for individual spermatozoa varies with time. Using STORM, we visualized individual *WT* sperm cells in heterogeneous populations 90 min after capacitation. While the intensity of P-CaMKII and caveolin-1 in the quadrilateral structure was reduced, the majority of proteins were not delocalized (Figure 6C, D; Figure S7F, G). The reduced protein level of PP2B-Aγ is manifest in the partial loss of the quadrilateral structure (Figure 6C, D; Figure S7F, G). As expected, the population variability (Figure 6D) was not observed when protein levels were relatively constant during capacitation (e.g., CatSperδ, GLUT3; Figure S7A–D). In some cells, CaMKII (P-T286) and CatSper1 signals now appear near the axoneme (Figure 6C, D; Figure S7G). The asymmetric molecular distribution across individual flagella may be reflected in the well known individual variation in sperm motility 90 min after capacitation (Neill and Olds-Clarke, 1987).

Hyperactivating Spermatozoa Are Recognized by their Intact CatSper Ca^{2+} Domains

To correlate molecular changes with sperm behavior, we performed motility-correlation 3D STORM imaging of sperm cells. Sperm were placed on photo-etched grid coverslips, *in vitro* capacitated, and their motion recorded (Figure 6E; Movie S2). During subsequent immunostaining, many hyperactivated spermatozoa detached, but the remaining spermatozoa could be back-correlated to video-recorded activity via fiduciary marks. Before sperm cells capacitated, CatSper domains were intact without apparent P-Tyr in the tail (Figure 2G; Figure 4A). After 90 min capacitation, the number of CatSper domains and their organization varied (Figure 6D). Most important, we found that all spermatozoa displaying hyperactivated motility maintained their quadrilateral CatSper Ca^{2+} domains and were tyrosine phosphorylated (Figure 6D–F). In contrast, in some of the non-motile cells examined, CatSper domains degraded and were no longer specifically confined to the principle piece (Figure 6F). We conclude that intact CatSper domains and focused P-Tyr are required for sustained hyperactivated motility and successful fertilizing capacity.

CatSper is Required for Efficient Sperm Migration in the Oviduct

Thus far, our results suggest that a population of *in vitro* capacitated sperm represent both intact and degenerating and/or non-fertilizing spermatozoa. We thus examined *in vivo* migration of *WT* and *CatSper1-null* spermatozoa in the female mouse reproductive tract. *CatSper1-null* spermatozoa were crossed with Acr-EGFP Su9-DsRed2 mice (Hasuwa et al., 2010) to enhance sperm detection. Sperm migration from the uterus into the oviduct first

appeared ~1.5-h post-coitus in both *WT* and *CatSper1-null* mice, with more *WT* spermatozoa passing through the utero-tubal junction (UTJ) (Figure S7H). By 3-h after copulation, there were substantially fewer *CatSper1-null* than *WT* spermatozoa in the isthmus (Figure 6I; I1–2; Figure 6H; H1–2). Once in the oviduct, *CatSper* null sperm might less effectively detach from the epithelium (Ho et al., 2009) and rheotax in the oviductal flow (Miki and Clapham, 2013) for migration to the ampulla [4–5-h after copulation, ~10 *WT* spermatozoa reach the ampullae (Miki and Clapham, 2013)]. Similar numbers of *CatSper1-null* spermatozoa are not present until 8-h after coitus, at a time when hundreds of WT spermatozoa are detected (Figure S7I). Thus, a primary cause of *CatSper1-null* male sterility is inefficient migration past the UTJ to the fertilizing site. *CatSper* null spermatozoa also have lower basal levels of [Ca^{2+}] (Marquez et al., 2007) and ATP (Xia et al., 2007), but higher levels of cAMP (Carlson et al., 2005). These phenotypes may contribute to the relatively rapid loss of overall motility observed in *CatSper* null spermatozoa during capacitation (Qi et al., 2007).

DISCUSSION

Sperm Calcium Channels are in a Highly Organized Ca^{2+} Distribution Network

Ca^{2+} is a highly localized second messenger. Subcellular compartments, such as the endoplasmic reticulum and mitochondria, tightly control its entry and spread within a cell. In areas of close apposition between cells, such as neuronal and immunological synapses, molecules are arranged to further restrict and define calcium concentrations (Clapham, 2007). In the sperm principal piece, which lacks ER and mitochondria, there is an especially high level of organization of molecular structures governing calcium signaling. This may control and coordinate Ca^{2+} signaling along the extremely long (>100-ɛm) and narrow (<1-ɛm) tail in hyperactivated motility. The compartmentalized organization should serve to focus signaling, generating stronger and faster engagement of effectors. Since sperm rotate about their longitudinal axis as they rheotax (Miki and Clapham, 2013), the multi-linear arrangement may conserve space and enhance detection of finite signals. In contrast, transporters such as PMCA4 and Glut3, with 10^3-fold slower kinetics than ion channels, are not compartmentalized, and occupy the maximum surface area possible. As a novel structural feature in the sperm of marsupial and eutherian mammals, the fibrous sheath defines the principal piece of the flagellum (Eddy, 2007). The fibrous sheath replaces the outer dense fibers just under the longitudinal column and directly attaches to the #3 and #8 microtubule doublets. Localization of CatSper alongside the longitudinal columns may alter the flexibility of the longitudinal columns or spatially regulate microtubule doublets. Nevertheless, it is clear that CatSper Ca^{2+} domains orchestrate the timing and extent of complex phosphorylation cascades. These cascades ultimately alter axonemal motion to initiate the characteristic asymmetric and high angle bend of hyperactivated motility. It will be of particular interest to determine whether any of these sites is phosphorylated/dephosphorylated asymmetrically along and/or across the axoneme as hyperactivation develops.

Spatiotemporal Control of Sperm Tyrosine Phosphorylation

Protein tyrosine phosphorylation, normally maintained until egg interaction (Sakkas et al., 2003; Urner et al., 2001), is recognized as the primary biochemical signature of capacitation.

Even after extended capacitation, most P-Tyr is concentrated in the axoneme. Surprisingly, disruption of CatSper results in an increase and mislocalization of P-Tyr, beginning in the axoneme and spreading into the peri-axonemal regions. Abrogation of *CatSper* also resulted in the loss of temporal organization of P-Tyr. Many observations in sperm physiology have been restricted to detection using immunoblotting, diffraction-limited images from conventional optical imaging or sectioned images from immuno-EM. Previous diverse conclusions regarding Ca^{2+} regulation of sperm P-Tyr development may mirror kinetic and spatial complexity. Super-resolution fluorescence imaging at higher time resolution would help reconcile these disparate results.

Protein Tyrosine Phosphorylation in Sperm Structure and Metabolism

Two decades after the recognition of capacitation associated P-Tyr (Visconti et al., 1995a), there is still limited information about the kinases, their targets, and their effects on sperm function. Here, we report 62 P-Tyr peptides on 45 proteins common to both *WT* and *CatSper1-null* spermatozoa, the most comprehensive list of P-Tyr sperm proteins to date. Not surprisingly for a flagellum, 23 P-Tyr sites were identified on 12 structural proteins in the annulus, axoneme, and peri-axoneme. Capacitation increased tyrosine phosphorylation more than 2-fold in 11 of these proteins in a CatSper-dependent manner. It is intriguing that radial spoke head protein 3 homolog A (Rshph3a) is among the P-Tyr structure proteins since radial spoke proteins are prime candidates for bend angle changes in flagellated organisms (Porter and Sale, 2000).

Hyperactivated motility generates more force but demands more flagellar glycolysis in the fibrous sheath (Eddy, 2007). Mitochondria are compartmentalized in the midpiece and are not necessary for prolonged flagellar activity (Mukai and Okuno, 2004). We found that capacitation induces P-Tyr of 9 peptides on 6 metabolic proteins. Cytosolic 5’ nucleotidase 1b (Nt5C1b) dephosphorylates the 5’ and 2’(3’)-phosphates of deoxynucleotides to regulate adenosine levels (Sala-Newby and Newby, 2001). All 3 localized sites on Nt5C1b peptides increase P-Tyr level significantly in *CatSper1-null* spermatozoa. The reduced basal ATP levels in *CatSper* null spermatozoa (Xia et al., 2007) and the augmented protein phosphorylation upon capacitation could stem from activity changes induced by P-Tyr of these sites. Although not investigated here, we propose that the CatSper distribution system supports the increased ATP requirements during hyperactivation. The fibrous sheath that separates the axoneme from the plasma membrane houses testis-specific Ca^{2+}-binding proteins such as CABYR and FSCB (Li et al., 2007; Naaby-Hansen et al., 2002). As endogenous buffers, they could limit changes in the intraflagellar $[Ca^{2+}]$, or be Ca^{2+}-dependent adaptors to metabolic enzymes such as fibrous sheath-localized GAPDHs and LDH (Krisfalusi et al., 2006; Miki et al., 2004).

CatSper as a Countdown Timer

Uniflagellated parasites persist for long durations within a host, an outcome that would be detrimental if sperm cells had the same capability. On the other hand, some spermatozoa can survive for days (humans), weeks (bats), or months (crocodiles) in oviductal crypts (Birkhead, 1993). We showed that in mice, caveolin-1, P-CaMKII, and calcineurin (PP2B-Aγ) are reduced and CatSper1 is processed 90 min after capacitation. We propose that these

changes set sperm lifetime and eventually signal the end of motility. Exceptionally few (~5–20 of 5–20 million) spermatozoa reach the egg at the time of fertilization, and perhaps selection factors initiate the demise of most spermatozoa. Continuation of hyperactivated motility requires the maintenance of the CatSper domains and focused P-Tyr at the axoneme. Other sperm might have reached their expiration date by virtue of degradation of CatSper domain components, limiting their potential to fertilize ectopic eggs or migrate into the peritoneum.

Future areas for investigation are the precise timing of phosphorylation events, the identity of the substrates of CaMKII and calcineurin in the Ca^{2+} signaling domain, and the detailed links between Ca^{2+} signaling and capacitation-associated PKA-dependent protein tyrosine phosphorylation. The novel P-Tyr sites identified in the study will serve as a foundation to this end.

Experimental Procedures

Full details are provided in the Extended Experimental Procedures. Mice were treated in accordance with guidelines approved by the Boston Children's Hospital Animal Care and Use Committee (IUACUC).

Spermatozoa Preparation and *in vitro* Capacitation

Mouse caudal epididymal sperm were collected by swim-out in HEPES buffered saline (HS) (Chung, 2011). To induce capacitation *in vitro*, sperm cells were incubated (2×10^6 cells ml^{-1}) in human tubular fluid (HTF) media (Millipore) for 90 min at 37°C (5% CO^2).

Stochastic Optical Reconstruction Microcopy (STORM) Imaging

3D STORM experiments were performed as previously described (Huang et al., 2008a; Huang et al., 2008b). Imaging buffer was prepared in 60% (wt/wt) sucrose solution, increasing imaging depth to ~1 ɛm (Huang et al., 2008a). Imaging buffer was supplemented with 100 mM mercaptoethylamine (pH 8.5) as a switching agent as well as an O_2 scavenger (5% glucose (wt/vol), 0.5 mg/mL glucose oxidase and 40 mg/mL catalase) to prevent photobleaching. The sample was illuminated at 657-nm for imaging, and 405 or 532-nm to reactivate the dye in order to excite and switch off the reporter dye, Alexa 647. For 3D localization, a cylindrical lens (focal length = 1 m) was inserted into the detection path to enable determination of *z*-positions from the ellipticities of the molecular images and the *x*- and *y*-positions from the centroid positions (Huang et al., 2008b). In 2-color imaging, the two targets were immunolabeled with photoswitchable dye pairs: one with Alexa405 and Alexa647; another with Cy3 and Alexa647. Then, an illumination sequence of one frame of activation illumination (405 nm for Alexa405 or 532 nm for Cy3) followed by 3 frames of imaging illumination (657 nm) was used to identify the targets by the wavelength of activation lasers (Bates et al., 2007; Huang et al., 2008a).

P-Tyr Peptide Affinity Purification with Tandem Mass Tagging

Urea-digested lysates of capacitated mouse sperm cells (triplicates) were reduced, alkylated, digested with trypsin and reverse-phase purified (Villen and Gygi, 2008). Phosphopeptides

were enriched using TiO_2 and TMT-labeled; *WT* (126, 127, and 128) and *KO* (129, 130, 131) (Pierce). The non-phosphorylated peptides from the flow-through were also TMT-labeled and used for protein quantitation. After labeling, the phospho-enriched samples were combined and purified using tC18 Sep-Pak (Waters) and dried. The combined sample was reconstituted and bound to phosphotyrosine (pY) 1000-bead slurry (Cell Signaling Technology). P-Tyr peptides were eluted, and analyzed (see Extended Experimental Procedures). The sample was acquired on an Orbitrap Fusion Tribrid mass spectrometer (Thermo Scientific) using an MS^3 method. The Sequest search engine (Thermo Scientific) was used to match MS/MS spectra to peptides; the false discovery rate was controlled to 1% at the peptide and protein level. Site localization confidence was assessed using the Ascore algorithm. Peptides having a sum of the TMT reporter ion signal/noise ≥ 65 were used for quantitation. For complete details, data may be downloaded from the Chorusproject.org network. The specific Chorus key for the dataset is listed in the Extended Experimental Procedures.

Supplementary Material

Refer to Web version on PubMed Central for supplementary material.

Acknowledgments

We thank K. Miki, B. Navarro for discussions, L. Zhao, Y. Shang, and H. Warren for help with mice and western blots, and M. Ericsson and E. Benecchi at the Harvard Medical School EM facility for assistance with electron microscopy. This work was supported by NIH U01 HDO45857 (to D.E.C) and by NIH 1R01 GM 068518 and 1R01 GM 096450 (to X.Z.).

REFERENCES

Amanchy R, Periaswamy B, Mathivanan S, Reddy R, Tattikota SG, Pandey A. A curated compendium of phosphorylation motifs. Nat Biotechnol. 2007; 25:285–286. [PubMed: 17344875]

Avenarius MR, Hildebrand MS, Zhang Y, Meyer NC, Smith LL, Kahrizi K, Najmabadi H, Smith RJ. Human male infertility caused by mutations in the CATSPER1 channel protein. Am J Hum Genet. 2009; 84:505–510. [PubMed: 19344877]

Avidan N, Tamary H, Dgany O, Cattan D, Pariente A, Thulliez M, Borot N, Moati L, Barthelme A, Shalmon L, et al. CATSPER2, a human autosomal nonsyndromic male infertility gene. Eur J Hum Genet. 2003; 11:497–502. [PubMed: 12825070]

Baldi E, Casano R, Falsetti C, Krausz C, Maggi M, Forti G. Intracellular calcium accumulation and responsiveness to progesterone in capacitating human spermatozoa. J Androl. 1991; 12:323–330. [PubMed: 1765568]

Ballif BA, Carey GR, Sunyaev SR, Gygi SP. Large-scale identification and evolution indexing of tyrosine phosphorylation sites from murine brain. J Proteome Res. 2008; 7:311–318. [PubMed: 18034455]

Bates M, Huang B, Dempsey GT, Zhuang X. Multicolor super-resolution imaging with photoswitchable fluorescent probes. Science. 2007; 317:1749–1753. [PubMed: 17702910]

Battistone MA, Da Ros VG, Salicioni AM, Navarrete FA, Krapf D, Visconti PE, Cuasnicu PS. Functional human sperm capacitation requires both bicarbonate-dependent PKA activation and downregulation of Ser/Thr phosphatases by Src family kinases. Mol Hum Reprod. 2013; 19:570–580. [PubMed: 23630234]

Birkhead TR, Moller AP. Sexual selection and the temporal separation of reproductive events: sperm storage data from reptiles, birds and mammals. Biological Journal of the Linnean Society. 1993; 50:295–311.

Carlson AE, Quill TA, Westenbroek RE, Schuh SM, Hille B, Babcock DF. Identical phenotypes of CatSper1 and CatSper2 null sperm. J Biol Chem. 2005; 280:32238–32244. [PubMed: 16036917]

Chang MC. Fertilizing capacity of spermatozoa deposited into the fallopian tubes. Nature. 1951; 168:697–698. [PubMed: 14882325]

Chen Y, Cann MJ, Litvin TN, Iourgenko V, Sinclair ML, Levin LR, Buck J. Soluble adenylyl cyclase as an evolutionarily conserved bicarbonate sensor. Science. 2000; 289:625–628. [PubMed: 10915626]

Chung JJ, Navarro B, Krapivinsky G, Krapivinsky L, Clapham DE. A novel gene required for male fertility and functional CATSPER channel formation in spermatozoa. Nature communications. 2011; 2:153.

Clapham DE. Calcium signaling (2007). Cell. 2007; 131:1047–1058. [PubMed: 18083096]

Corti C, Leclerc L'Hostis E, Quadroni M, Schmid H, Durussel I, Cox J, Dainese Hatt P, James P, Carafoli E. Tyrosine phosphorylation modulates the interaction of calmodulin with its target proteins. Eur J Biochem. 1999; 262:790–802. [PubMed: 10411641]

Craig AW, Zirngibl R, Williams K, Cole LA, Greer PA. Mice devoid of fer protein-tyrosine kinase activity are viable and fertile but display reduced cortactin phosphorylation. Mol Cell Biol. 2001; 21:603–613. [PubMed: 11134346]

Crooks GE, Hon G, Chandonia JM, Brenner SE. WebLogo: a sequence logo generator. Genome Res. 2004; 14:1188–1190. [PubMed: 15173120]

Dephoure N, Gould KL, Gygi SP, Kellogg DR. Mapping and analysis of phosphorylation sites: a quick guide for cell biologists. Mol Biol Cell. 2013; 24:535–542. [PubMed: 23447708]

Eddy, EM. The Scaffold role of the fibrous sheath. In: Roldan, ERS.; Gomendio, M., editors. Spermatology. Nottingham: Nottingham University Press; 2007. p. 45-62.

Eddy EM, Toshimori K, O'Brien DA. Fibrous sheath of mammalian spermatozoa. Microsc Res Tech. 2003; 61:103–115. [PubMed: 12672126]

Fawcett DW. A comparative view of sperm ultrastructure. Biol Reprod. 1970; 2(Suppl 2):90–127. [PubMed: 5521054]

Fawcett DW. The mammalian spermatozoon. Dev Biol. 1975; 44:394–436. [PubMed: 805734]

Hasuwa H, Muro Y, Ikawa M, Kato N, Tsujimoto Y, Okabe M. Transgenic mouse sperm that have green acrosome and red mitochondria allow visualization of sperm and their acrosome reaction in vivo. Exp Anim. 2010; 59:105–107. [PubMed: 20224175]

Heintzmann R, Gustafsson MGL. Subdiffraction resolution in continuous samples. Nat Photonics. 2009; 3:362–364.

Hell SW. Microscopy and its focal switch. Nat Methods. 2009; 6:24–32. [PubMed: 19116611]

Ho HC, Granish KA, Suarez SS. Hyperactivated motility of bull sperm is triggered at the axoneme by Ca2+ and not cAMP. Dev Biol. 2002; 250:208–217. [PubMed: 12297107]

Ho K, Wolff CA, Suarez SS. CatSper-null mutant spermatozoa are unable to ascend beyond the oviductal reservoir. Reprod Fertil Dev. 2009; 21:345–350. [PubMed: 19210926]

Hornbeck PV, Chabra I, Kornhauser JM, Skrzypek E, Zhang B. PhosphoSite: A bioinformatics resource dedicated to physiological protein phosphorylation. Proteomics. 2004; 4:1551–1561. [PubMed: 15174125]

Huang B, Babcock H, Zhuang X. Breaking the diffraction barrier: super-resolution imaging of cells. Cell. 2010; 143:1047–1058. [PubMed: 21168201]

Huang B, Jones SA, Brandenburg B, Zhuang X. Whole-cell 3D STORM reveals interactions between cellular structures with nanometer-scale resolution. Nat Methods. 2008a; 5:1047–1052. [PubMed: 19029906]

Huang B, Wang W, Bates M, Zhuang X. Three-dimensional super-resolution imaging by stochastic optical reconstruction microscopy. Science. 2008b; 319:810–813. [PubMed: 18174397]

Hudmon A, Schulman H. Structure-function of the multifunctional Ca2+/calmodulin-dependent protein kinase II. Biochem J. 2002; 364:593–611. [PubMed: 11931644]

Jaiswal BS, Conti M. Calcium regulation of the soluble adenylyl cyclase expressed in mammalian spermatozoa. Proc Natl Acad Sci U S A. 2003; 100:10676–10681. [PubMed: 12958208]

Johnson LR, Foster JA, Haig-Ladewig L, VanScoy H, Rubin CS, Moss SB, Gerton GL. Assembly of AKAP82, a protein kinase A anchor protein, into the fibrous sheath of mouse sperm. Dev Biol. 1997; 192:340–350. [PubMed: 9441672]

Kierszenbaum AL, Rivkin E, Tres LL. Expression of Fer testis (FerT) tyrosine kinase transcript variants and distribution sites of FerT during the development of the acrosome-acroplaxome-manchette complex in rat spermatids. Dev Dyn. 2008; 237:3882–3891. [PubMed: 18985748]

Kirichok Y, Navarro B, Clapham DE. Whole-cell patch-clamp measurements of spermatozoa reveal an alkaline-activated Ca2+ channel. Nature. 2006; 439:737–740. [PubMed: 16467839]

Krapf D, Arcelay E, Wertheimer EV, Sanjay A, Pilder SH, Salicioni AM, Visconti PE. Inhibition of Ser/Thr phosphatases induces capacitation-associated signaling in the presence of Src kinase inhibitors. J Biol Chem. 2010; 285:7977–7985. [PubMed: 20068039]

Krisfalusi M, Miki K, Magyar PL, O'Brien DA. Multiple glycolytic enzymes are tightly bound to the fibrous sheath of mouse spermatozoa. Biol Reprod. 2006; 75:270–278. [PubMed: 16687649]

Li YF, He W, Jha KN, Klotz K, Kim YH, Mandal A, Pulido S, Digilio L, Flickinger CJ, Herr JC. FSCB, a novel protein kinase A-phosphorylated calcium-binding protein, is a CABYR-binding partner involved in late steps of fibrous sheath biogenesis. J Biol Chem. 2007; 282:34104–34119. [PubMed: 17855365]

Lin Y, Kan FW. Regionalization and redistribution of membrane phospholipids and cholesterol in mouse spermatozoa during in vitro capacitation. Biol Reprod. 1996; 55:1133–1146. [PubMed: 8902227]

Liu J, Xia J, Cho KH, Clapham DE, Ren D. CatSperbeta, a novel transmembrane protein in the CatSper channel complex. J Biol Chem. 2007; 282:18945–18952. [PubMed: 17478420]

Marquez B, Ignotz G, Suarez SS. Contributions of extracellular and intracellular Ca2+ to regulation of sperm motility: Release of intracellular stores can hyperactivate CatSper1 and CatSper2 null sperm. Dev Biol. 2007; 303:214–221. [PubMed: 17174296]

Miki K, Clapham DE. Rheotaxis guides mammalian sperm. Curr Biol. 2013; 23:443–452. [PubMed: 23453951]

Miki K, Qu W, Goulding EH, Willis WD, Bunch DO, Strader LF, Perreault SD, Eddy EM, O'Brien DA. Glyceraldehyde 3-phosphate dehydrogenase-S, a sperm-specific glycolytic enzyme, is required for sperm motility and male fertility. Proc Natl Acad Sci U S A. 2004; 101:16501–16506. [PubMed: 15546993]

Mukai C, Okuno M. Glycolysis plays a major role for adenosine triphosphate supplementation in mouse sperm flagellar movement. Biol Reprod. 2004; 71:540–547. [PubMed: 15084484]

Muramatsu T, Giri PR, Higuchi S, Kincaid RL. Molecular cloning of a calmodulin-dependent phosphatase from murine testis: identification of a developmentally expressed nonneural isoenzyme. Proc Natl Acad Sci U S A. 1992; 89:529–533. [PubMed: 1309945]

Naaby-Hansen S, Mandal A, Wolkowicz MJ, Sen B, Westbrook VA, Shetty J, Coonrod SA, Klotz KL, Kim YH, Bush LA, et al. CABYR, a novel calcium-binding tyrosine phosphorylation-regulated fibrous sheath protein involved in capacitation. Dev Biol. 2002; 242:236–254. [PubMed: 11820818]

Neill JM, Olds-Clarke P. A computer-assisted assay for mouse sperm hyperactivation demonstrates that bicarbonate but not bovine serum albumin is required. Gamete Res. 1987; 18:121–140. [PubMed: 3507366]

Patterson G, Davidson M, Manley S, Lippincott-Schwartz J. Superresolution Imaging using Single-Molecule Localization. Annu Rev Phys Chem. 2010; 61:345–367. [PubMed: 20055680]

Porter ME, Sale WS. The 9 + 2 axoneme anchors multiple inner arm dyneins and a network of kinases and phosphatases that control motility. J Cell Biol. 2000; 151:F37–F42. [PubMed: 11086017]

Qi H, Moran MM, Navarro B, Chong JA, Krapivinsky G, Krapivinsky L, Kirichok Y, Ramsey IS, Quill TA, Clapham DE. All four CatSper ion channel proteins are required for male fertility and sperm cell hyperactivated motility. Proc Natl Acad Sci U S A. 2007; 104:1219–1223. [PubMed: 17227845]

Quill TA, Sugden SA, Rossi KL, Doolittle LK, Hammer RE, Garbers DL. Hyperactivated sperm motility driven by CatSper2 is required for fertilization. Proc Natl Acad Sci U S A. 2003; 100:14869–14874. [PubMed: 14657366]

Razani B, Engelman JA, Wang XB, Schubert W, Zhang XL, Marks CB, Macaluso F, Russell RG, Li M, Pestell RG, et al. Caveolin-1 null mice are viable but show evidence of hyperproliferative and vascular abnormalities. J Biol Chem. 2001; 276:38121–38138. [PubMed: 11457855]

Razani B, Woodman SE, Lisanti MP. Caveolae: from cell biology to animal physiology. Pharmacol Rev. 2002; 54:431–467. [PubMed: 12223531]

Ren D, Navarro B, Perez G, Jackson AC, Hsu S, Shi Q, Tilly JL, Clapham DE. A sperm ion channel required for sperm motility and male fertility. Nature. 2001; 413:603–609. [PubMed: 11595941]

Rust MJ, Bates M, Zhuang X. Sub-diffraction-limit imaging by stochastic optical reconstruction microscopy (STORM). Nat Methods. 2006; 3:793–795. [PubMed: 16896339]

Sakkas D, Leppens-Luisier G, Lucas H, Chardonnens D, Campana A, Franken DR, Urner F. Localization of tyrosine phosphorylated proteins in human sperm and relation to capacitation and zona pellucida binding. Biol Reprod. 2003; 68:1463–1469. [PubMed: 12606470]

Sala-Newby GB, Newby AC. Cloning of a mouse cytosolic 5'-nucleotidase-I identifies a new gene related to human autoimmune infertility-related protein. Biochim Biophys Acta. 2001; 1521:12–18. [PubMed: 11690631]

Schalles U, Shao X, van der Hoorn FA, Oko R. Developmental expression of the 84-kDa ODF sperm protein: localization to both the cortex and medulla of outer dense fibers and to the connecting piece. Dev Biol. 1998; 199:250–260. [PubMed: 9698445]

Schwartz D, Gygi SP. An iterative statistical approach to the identification of protein phosphorylation motifs from large-scale data sets. Nat Biotechnol. 2005; 23:1391–1398. [PubMed: 16273072]

Simpson IA, Dwyer D, Malide D, Moley KH, Travis A, Vannucci SJ. The facilitative glucose transporter GLUT3: 20 years of distinction. Am J Physiol Endocrinol Metab. 2008; 295:E242–E253. [PubMed: 18577699]

Smith JF, Syritsyna O, Fellous M, Serres C, Mannowetz N, Kirichok Y, Lishko PV. Disruption of the principal, progesterone-activated sperm Ca2+ channel in a CatSper2-deficient infertile patient. Proc Natl Acad Sci U S A. 2013; 110:6823–6828. [PubMed: 23530196]

Tash JS, Krinks M, Patel J, Means RL, Klee CB, Means AR. Identification, characterization, and functional correlation of calmodulin-dependent protein phosphatase in sperm. J Cell Biol. 1988; 106:1625–1633. [PubMed: 2836436]

Travis AJ, Merdiushev T, Vargas LA, Jones BH, Purdon MA, Nipper RW, Galatioto J, Moss SB, Hunnicutt GR, Kopf GS. Expression and localization of caveolin-1, and the presence of membrane rafts, in mouse and Guinea pig spermatozoa. Dev Biol. 2001; 240:599–610. [PubMed: 11784086]

Urner F, Leppens-Luisier G, Sakkas D. Protein tyrosine phosphorylation in sperm during gamete interaction in the mouse: the influence of glucose. Biol Reprod. 2001; 64:1350–1357. [PubMed: 11319138]

Villen J, Gygi SP. The SCX/IMAC enrichment approach for global phosphorylation analysis by mass spectrometry. Nat Protoc. 2008; 3:1630–1638. [PubMed: 18833199]

Visconti PE, Bailey JL, Moore GD, Pan D, Olds-Clarke P, Kopf GS. Capacitation of mouse spermatozoa. I. Correlation between the capacitation state and protein tyrosine phosphorylation. Development. 1995a; 121:1129–1137. [PubMed: 7743926]

Visconti PE, Moore GD, Bailey JL, Leclerc P, Connors SA, Pan D, Olds-Clarke P, Kopf GS. Capacitation of mouse spermatozoa. II. Protein tyrosine phosphorylation and capacitation are regulated by a cAMP-dependent pathway. Development. 1995b; 121:1139–1150. [PubMed: 7538069]

Williams AC, Ford WC. The role of glucose in supporting motility and capacitation in human spermatozoa. J Androl. 2001; 22:680–695. [PubMed: 11451366]

Xia J, Reigada D, Mitchell CH, Ren D. CATSPER channel-mediated Ca2+ entry into mouse sperm triggers a tail-to-head propagation. Biol Reprod. 2007; 77:551–559. [PubMed: 17554080]

Yanagimachi, R. Mammalian Fertilization. In: Knobil, EN.; D, J., editors. The Physiology of Reproduction. New York: Raven Press; 1994. p. 189-317.

Zeng XH, Navarro B, Xia XM, Clapham DE, Lingle CJ. Simultaneous knockout of Slo3 and CatSper1 abolishes all alkalization-and voltage-activated current in mouse spermatozoa. J Gen Physiol. 2013; 142:305–313. [PubMed: 23980198]

Highlights

- The sperm Ca^{2+} channel, CatSper, organizes 4-fold linear Ca^{2+} signaling domains
- The Ca^{2+} signaling domains focus protein phosphorylation in time and space
- Intact CatSper Ca^{2+} signaling domains time sperm hyperactivation
- CatSper enables efficient sperm migration in the female reproductive tract

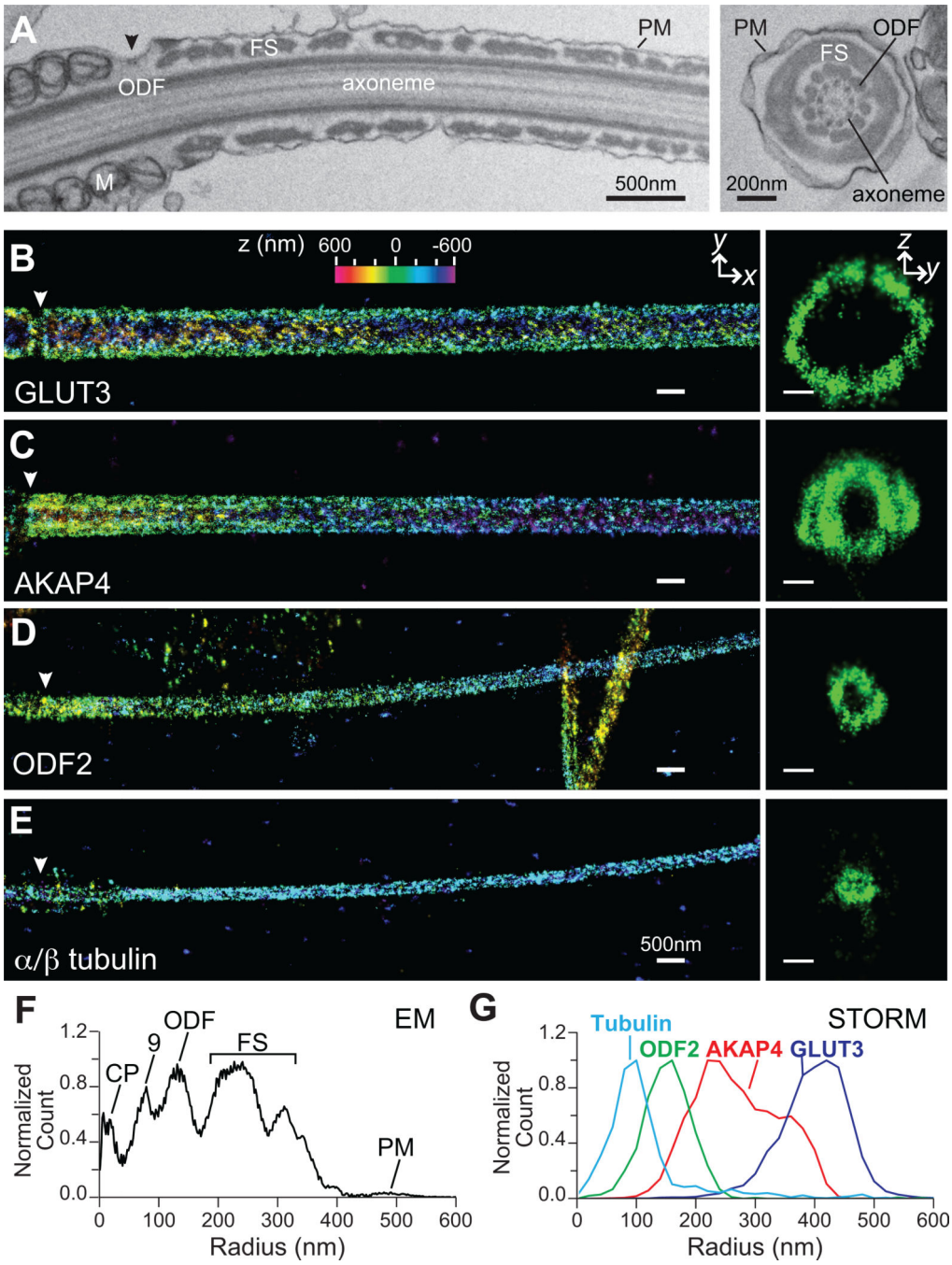

Figure 1. 3D STORM reproduces known structures in the sperm flagella

(**A**) Reference transmission electron micrographs. *Left*; longitudinal section (10,000×) near the annulus (arrowhead). *Right*: cross-section of principal piece (12,000×). *FS*, fibrous sheath; *ODF*, outer dense fibers; *PM*, plasma membrane; *M*, mitochondria. (**B–E**) 3D STORM images of (**B**) Glucose transporter 3 (GLUT3), (**C**) A-kinase anchoring protein 4 (AKAP4), (**D**) Outer dense fiber 2 (ODF2; V-shaped large structure is from other sperm tails), and (**E**) α/β-tubulin. *Left*, *x-y* projections. *Right*, *y-z* cross-sections near the annulus (white arrowheads). The color in all *x-y* projections encodes the relative distance from the

focal plane along the z-axis (color scale bar in B). (**F–G**) Radial profiles of (**F**) TEM cross-section in A; and (**G**) STORM cross-sections in B–E. *CP*, central pair of microtubules; *9*, 9 outer doublets of microtubules. See also Figure S1.

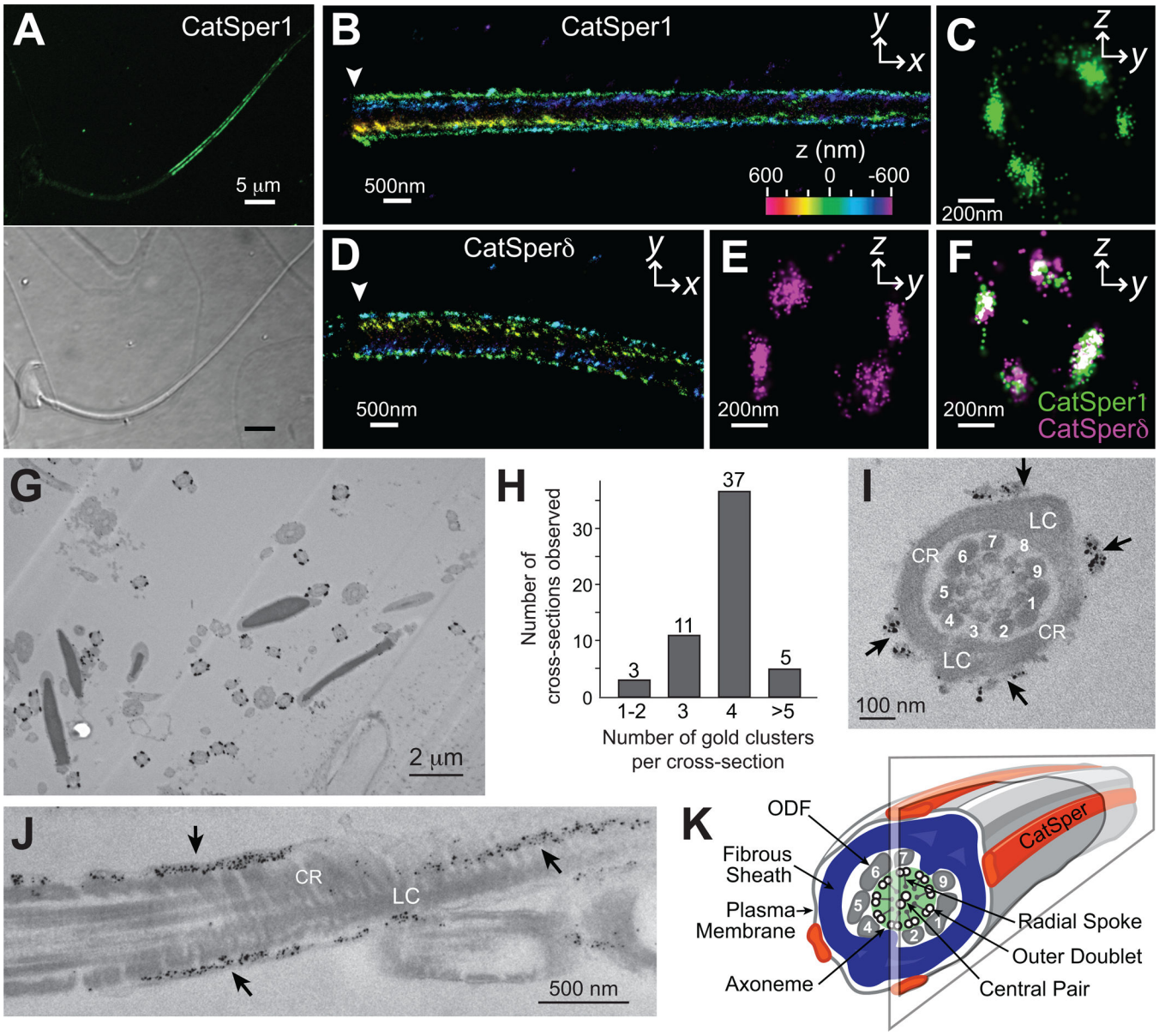

Figure 2. CatSper proteins form four linear domains

Each domain runs along each side of the longitudinal columns of the sperm flagella. (**A**) Confocal fluorescence (*upper*) and the corresponding phase-contrast (*lower*) images of immunostained CatSper1 in mouse sperm. (**B–E**) 3D STORM images of CatSper1 in *x-y* projection (**B**), in *y-z* cross-section (**C**), CatSperδ in *x-y* projection (**D**), and in *y-z* cross-section (**E**) at the initiation of the principal piece (white arrowhead). Colors in B and D indicate the *z*-positions (see color scale bar in B). See also Movie S1. (**F**) Co-localization of CatSper1 (green) and CatSperδ (magenta). (**G**) Silver-intensified immunogold electron microscope images of CatSper1 (3,000×). (**H**) CatSper gold clusters/cross-section from 3,000× images; n =56. Note that <4 clusters are only seen in smaller cross-sections of <500-nm diameter, reflecting attenuation of CatSper1 fluorescence in the distal region (A). (**I**) A magnified cross-section. *LC*, longitudinal column; *CR*, circumferential rib. Numbers indicate

ODFs corresponding to the microtubule pairs of the axoneme. (**J**) Off-center longitudinal section. Arrows indicate the Ag-intensified immunogold-labeled CatSper1. (**K**) Cartoon of the sperm flagellum showing the orientation of the EM section shown in I and J. The off-center cut is drawn to show the location of the linear arrangement of CatSper (red) captured in J relative to the underlying cytoskeletal structures. See also Figure S2.

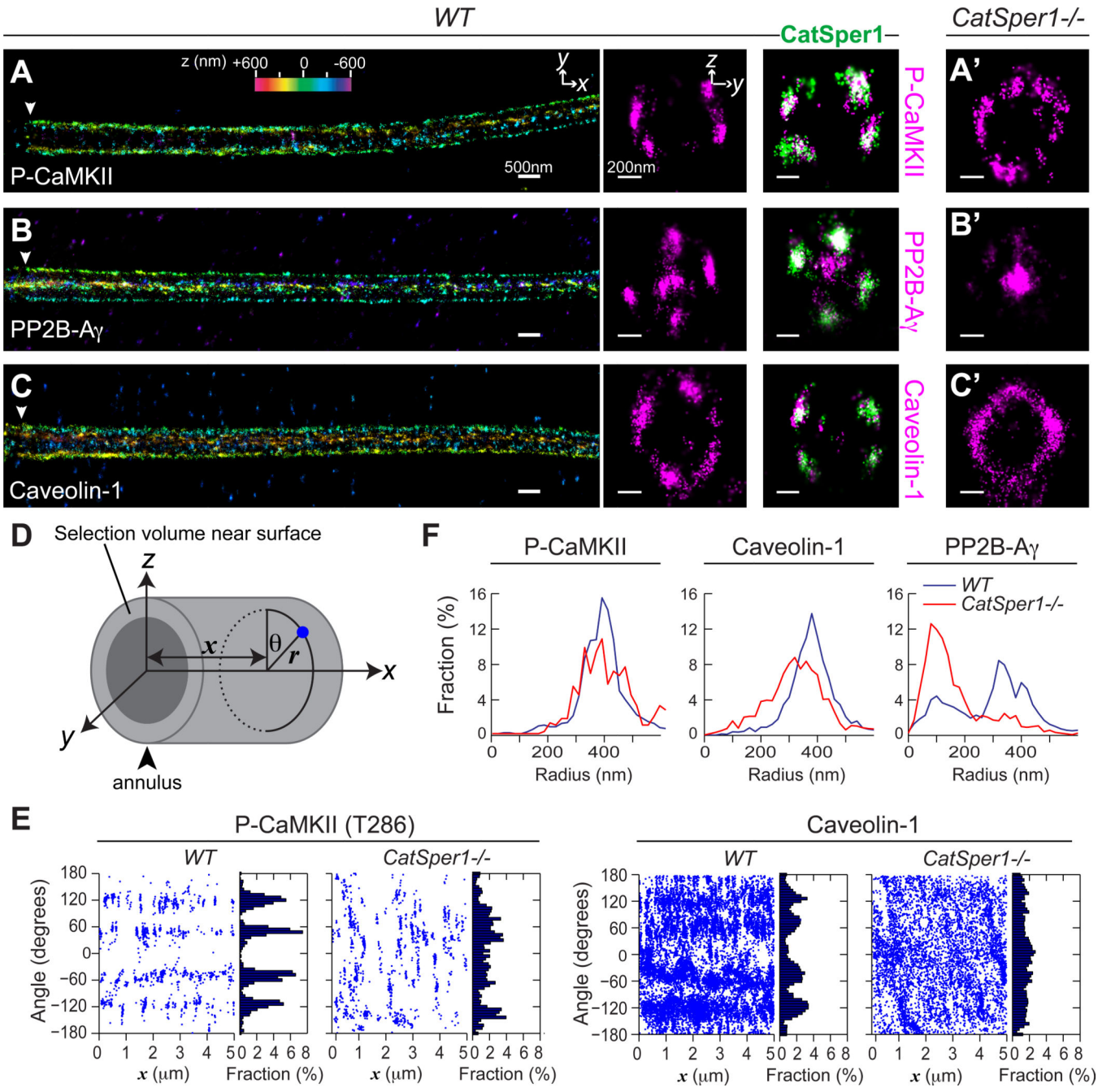

Figure 3. CatSper is essential to Ca^{2+} domain organization

(**A–C**) 3D STORM images of flagellar proteins: (**A**) CaMKII (P-T286), (**B**) Protein phosphatase 2B, catalytic subunit Aγ (PP2B-Aγ), and (**C**) caveolin-1. *Left*, *x-y* projections. Colors indicate z-positions (see color scale bar in A). *Middle*, *y-z* cross-sections near the annulus (white arrowheads). *Right*, 2-color STORM images of CatSper1 (green) and P-CaMKII/PP2B-Aγ/caveolin-1 (magenta). (**A'–C'**) Delocalization of P-CaMKII (T286) (**A'**), PP2B-Aγ (**B'**), and caveolin-1 (**C'**) in *CatSper1-null* spermatozoa. (**D**) Cartoon of the cylindrical coordinate system for defining the radius and angles of molecular coordinates in STORM images. The longitudinal axis (*x*) is placed at the flagellar center and the origin at

the annulus. (**E**) Angular distributions (*left*) and profiles (*right*) of the surface-localized P-CaMKII (T286) and caveolin-1 in *WT* and *CatSper1-null* sperm shown in A, A' and C, C'. (**F**) Radial profiles of P-CaMKII, caveolin-1, and PP2B-Aγ of WT (*blue*) and CatSper1-null (*red*) flagella shown in A, A'–C, C'. See also Figures S3 and S4.

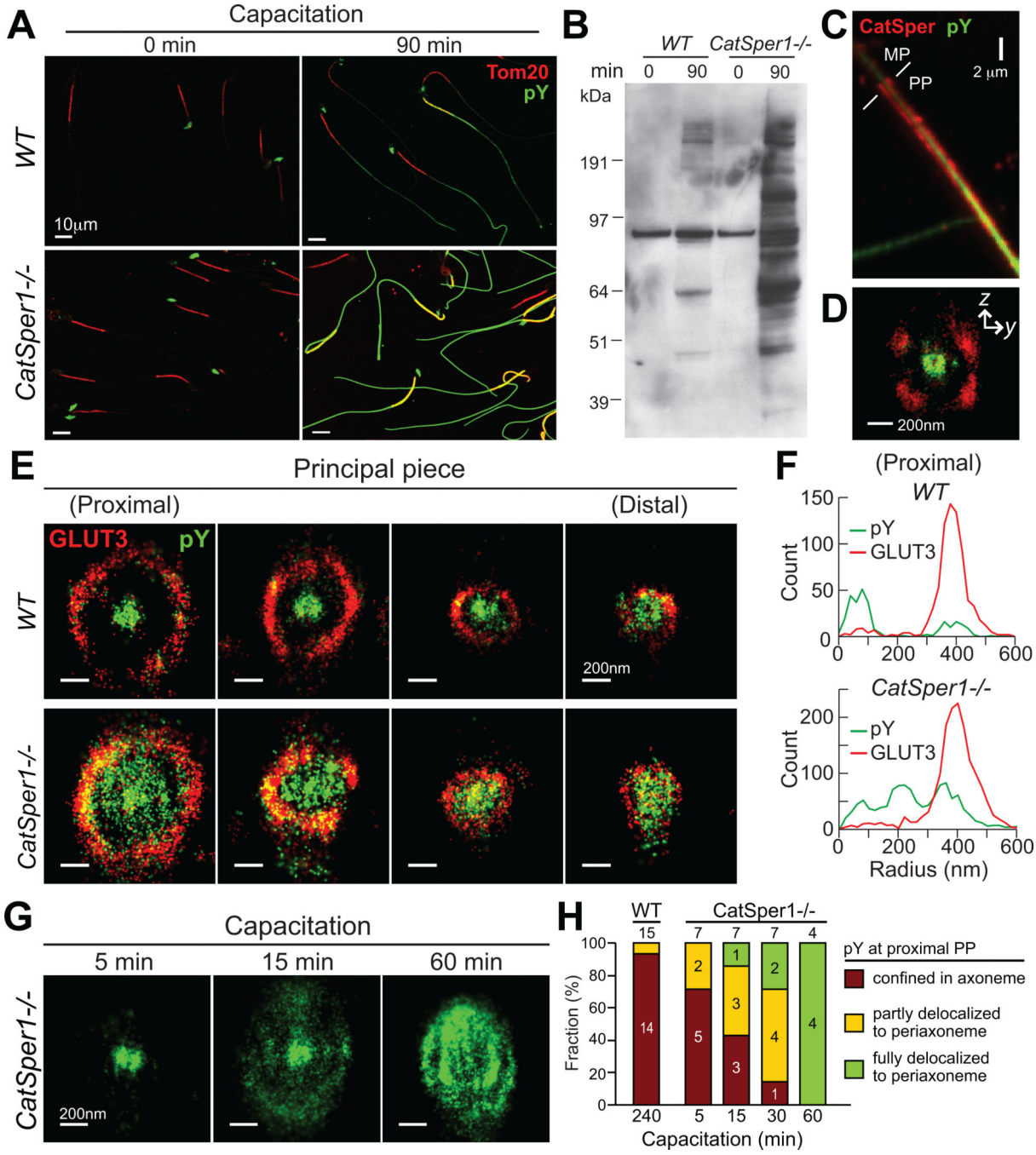

Figure 4. Ca^{2+} domains confine P-Tyr to the axoneme and inhibit premature P-Tyr

P-Tyr proteins are potentiated and delocalized in CatSper1-null spermatozoa. (**A**) Confocal fluorescence of P-Tyr (green) from mouse sperm incubated for the indicated time under capacitating conditions. Mitochondrial import receptor subunit, Tom20 (red), serves as reference for normalizing the intensity of P-Tyr under 4 different conditions. *Upper, WT; Lower, CatSper1-null* spermatozoa. (**B**) Immunoblot of total sperm cell extract by α-P-Tyr. (**C**) Fluorescence image of a capacitated WT spermatozoon co-immunostained by α-CatSper1 (red) and α-P-Tyr (green). *MP*, mid-piece. *PP*, principal piece. White lines mark

the boundary. (**D**) A 2-color STORM cross-section of CatSper1 (red) and P-Tyr (green) in a capacitated WT sperm cell. (**E**) Two-color STORM images of P-Tyr (green) and GLUT3 (red) in capacitated *WT* and *CatSper1-null* cells. The *y-z* cross-sections are obtained from the proximal to the distal part of the principal piece (same cells). (**F**) Radial profiles of pY (green) and GLUT3 (red) in the STORM cross-section in E. (**G**) STORM cross-sections of P-Tyr in *CatSper1-null* spermatozoa at different times during capacitation. (**H**) Time-course population variation of P-Tyr development in all spermatozoa imaged with 3D STORM. See also Figure S5.

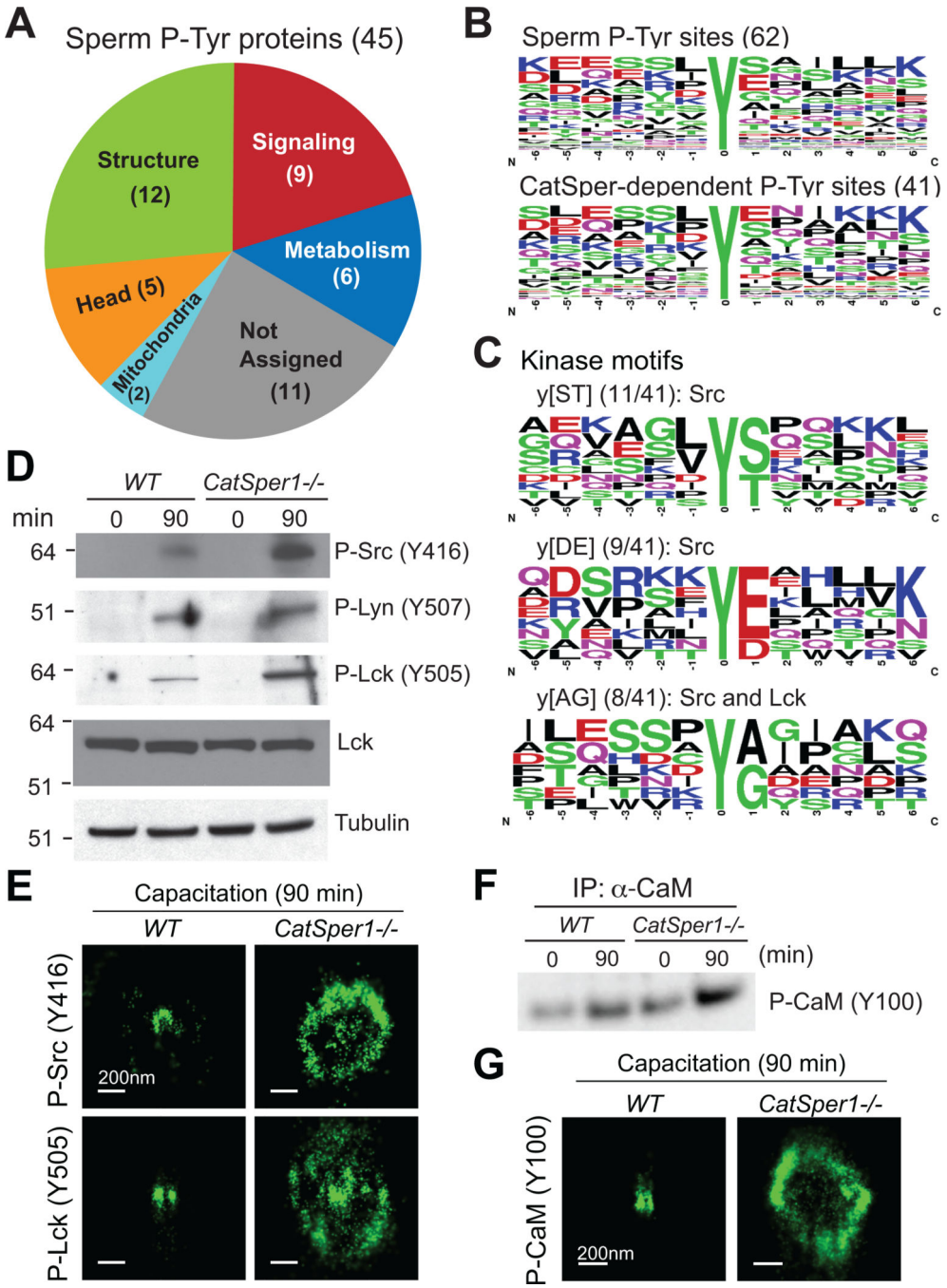

Figure 5. Profiling P-Tyr sites from capacitated sperm

Related to Figure S6, Tables S1 and S2. (**A**) Annotation of 45 P-Tyr proteins from capacitated *WT* and *CatSper1-null* spermatozoa. (**B**) Normalized amino acid frequency plots (WebLogo) for ± 6 residues neighboring all 62 tyrosine phosphorylation (P-Tyr) sites (*upper*) and 41 P-Tyr sites with the 2-fold ratio cutoff between *WT* and *CatSper1*-null spermatozoa (*lower*). (**C**) Kinase motifs extracted from the CatSper-dependent P-Tyr sites with P + 1 restriction. Three motifs (y[DE], y[AG], and y[ST]) fit to known Src consensus sites. Number of peptides for each given motif in parenthesis (see Table S2 for other motif

sequences with restriction on different positions). (**D**) Protein expression and phosphorylation of SFKs in sperm before (0-min) and after (90-min) capacitation. Recognition of P-Src (Y416), P-Lyn (Y507) and P-Lck (Y505). Lck and tubulin are loading controls. (**E**) STORM cross-sections of SFKs shown in D. (**F–G**) Validation of a pY target identified from this study. Expression (**F**) and sub-flagellar localization (**G**) of phosphorylated CaM at Y100 in capacitated (90-min) sperm.

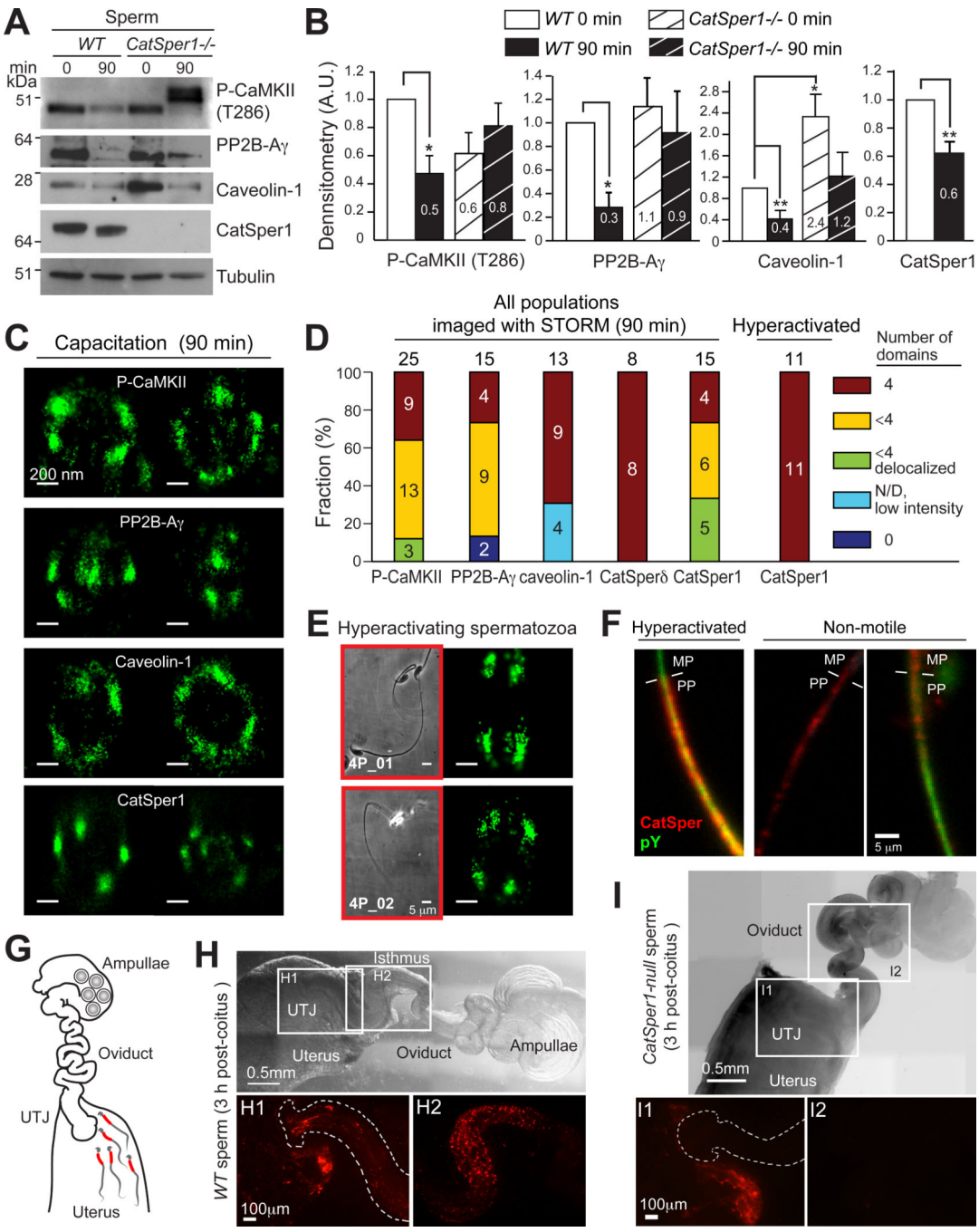

Figure 6. Sperm with intact CatSper domains hyperactivate and migrate efficiently

(**A–B**) Capacitation alters the levels of P-CaMKII, PP2B-A**γ**, caveolin-1 and CatSper1 in sperm. (**A**) Representative immunoblots from 3 – 4 experiments. (**B**) Relative densitometry of proteins in A. Signals normalized to tubulin and compared to uncapacitated sperm. Error bars denote s.e.m. of paired two-tailed ***t***-tests (***P**<0.05, ****P**<0.01). Protein declines after capacitation (*P*=0.013 for P-CaMKII, *P*=0.013 for PP2B-A**γ**, and *P*=0.009 for caveolin-1). Caveolin-1 is upregulated in *CatSper1-null* spermatozoa (*P*=0.014). (**C–D**) Capacitation generates heterogeneous molecular phenotypes. (**C**) Variation in sub-flagellar localization in

capacitated sperm; 2 representative 3D STORM cross-sections. (**D**) Population variation in structures of CatSper domain components in capacitated sperm. (**E**) Hyperactivated sperm have intact CatSper domains. Capacitated *WT* sperm cells on grid coverslips were videotaped for motility correlation, fixed and labeled for 3D STORM. Two representative hyperactivating sperm cells from grid 4P. *Left*, phase-contrast images. *Right*, STORM cross-sections of CatSper1. Also see Movie S2. (**F**) Confined P-Tyr in hyperactivated spermatozoa. 100× fluorescence images; CatSper1 (red) and P-Tyr (green). (**G–I**) Impaired sperm migration from the uterus into the oviduct in *CatSper1-null* mice. (**G**) Cartoon of sperm migration in the female. (**H–I**) Uterus and oviduct collected from *WT* females mated with DsRed2-tagged *WT* (**H**) and *CatSper1-null* (**I**) males 3-h after coitus. Two insets indicate areas including the end of uterus and uterotubal junction (UTJ, dotted line) (1) and the isthmus (2). See also Figure S7.

Table 1

Functional Categorization of Capacitated Sperm Proteins with Tyrosine Phosphorylation Sites

Category[a]	Symbol	Protein description	Position	Peptide sequence[b]	KO/WT[c]
Metabolism					
Energy	*Nt5c1b*	Cytosolic 5'-nucleotidase 1B, Isoform 2	175	DLQLRDY*AYSCDSR	13.6
			202	TPPTEWKPY*AQR	8.3
			548	FGTITAHVPY*GIAQK	6.8
	Hk1	Hexokinase-1, Isoform HK1-SB	31	YLY*AMR	0.8
	Gsk3a	Glycogen synthase kinase-3 alpha	279	GEPNVSY*ICSR	0.9
	Pgam2	Phosphoglycerate mutase 2	92	HY*GGLTGLNK	0.6
Lipid	*Dbil5*	Diazepam-binding inhibitor-like 5	56	AKY*EAWMVNK	3.4
		(Endozepine-like peptide)	74	IY*IAKVEELK	1.2
	Gpx4	Phospholipid hydroperoxide glutathione peroxidase, Isoform Cytoplasmic	96	EFAAGY*NVK	1.3
Signaling					
Ca^{2+}	*Calm1*	Calmodulin	100	DGNGY*ISAAELR	111.9
	Spa17	Sperm surface protein Sp17	69	VEDRFY*NNHAFK	9.5
	Fscb	Fibrous sheath CABYR-binding protein	73	KEY*ESLR	17.8
Kinases	*Prkar2a*	cAMP-dependent protein kinase type II-Alpha regulatory subunit	382	NISHY*EEQLVK	2.1
	Dyrk1a	Dual specificity tyrosine-phosphorylation-regulated kinase 1A	321	IYQY*IQSR	1.2
	Fer	Tyrosine-protein kinase Fer, Isoform 2	657	QEDGGVY*SSSGLK	1.2
Other	*Pebp1*	Phosphatidylethanolamine	181	LY*EQLSGK-	3.7
	Arrdc5	Arrestin domain	320	LDELPY*EDHMV-	1.2
	LRRD1	Leucine-rich repeat and death domain-containing protein 1	46	SKDSNQIY*EANPSK	1.2

Category[a]	Symbol	Protein description	Position	Peptide sequence[b]	KO/WT[c]
Structure					
Peri-axonemal	*Fsip2*	Fibrous sheath-interacting protein 2	630	TSLDY*QFPK	6.4
			1635	SLQSTLY*SHAK	3.9
			6101	ECQTASPY*TVQLPYK	4.7
			6351	VVNSVY*TNLLK	6.3
	Gm595	Novel protein (FSIP2-like)	472	Y*LYQNTK	2.9
			474	YLY*QNTK	5.7
			513	MFY*EPIQIK	4.2
	Akap3	A-kinase anchor protein 3	20	VGVY*SPGDNQHQDWK	4.3
			86	GFCVDY*YNTTNK	3.3
	Akap4	A-kinase anchor protein 4, Isoform 2	138	VGDLEGDY*SK	2.3
			292	TFLY*SEMCNK	4.1
			438	SQSLAY*ATLK	1.4
	Odf1	Outer dense fiber protein	82	LY*CLRPSLR	1.0
			154	KYSY*MNICK	2.5
			174	DVTY*SYGLGSCVK	1.0
			176	DVTYSY*GLGSCVK	1.0
	Axonemal	*Rsph3a*	Radial spoke head protein 3 homolog A	142	TAEASGLY*TYSSRPR	6.2
	Dnahc1	Dynein heavy chain 1, axonemal	18	EGPSSSSQGPGY*CPVKVPESHDLEK	5.3
	Dnali1	Axonemal Dynein light intermediate polypeptide 1 (inner dynein arm light chain)	11	Y*DTPVLVSR	2.4
	Spag17	Sperm-associated antigen 17 (PF6 homolog, central pair)	1785	EVTPY*FK	1.5
	Spatc1	Speriolin (sperm centrosome protein)	279	GNFSGTSAY*AGPAPTSK	24.2
	BC061194	Ortholog of H. sapiens sperm-associated antigen 6	493	YYSPGY*SDILLQR	1.5

Category[a]	Symbol	Protein description	Position	Peptide sequence[b]	KO/WT[c]
Annulus	*Gm11492*	C17orf47 homolog (Septin-4 isoform)	10	ATVY*QVYK	8.5
Head/Acrosome					
	Dydc1	DPY30 domain containing 1	150	TLAEISDRY*GAPNLSR	3.8
	Nsfl1c	NSFL1 cofactor p47, Isoform 3	169	LGAAPEEESAY*VAGERR	1.9
	Capza3	F-actin-capping protein subunit alpha-3	289	LGYVIY*SR	1.8
	Ubxn11	UBX domain-containing protein 11	56	ISLPSCY*GGIGAPVSR	7.3
	Tceb1	Transcription elongation factor B polypeptide 1 (SIII, Elongin-C)	8	TY*GGCEGPDAMYVK	1.9
Mitochondria					
	Spata18	Spermatogenesis associated 18 homolog, Isoform 3 (mitochondria-eating protein)	216	RTQDQRPQDVVSNY*EK	11.0
	Nadk2	Mitochondrial NAD kinase 2, isoform 3 (UPF0465 protein C5orf33 homolog)	96	GSSY*SGLLER	1.1
Uncharacterized					
	Ms4a14; *NYD-SP21*	membrane-spanning 4-domains, subfamily A, member 14 (CD20 domain)	455 457	DTSPQGTPY*QYILTK DTSPQGTPYQY*ILTK	12.4 6.4
	C2orf81	Uncharacterized protein C2orf81 homolog homologous to Dynactin 1)	237	VY*SPQSSLK	42.4
	C11orf35	Uncharacterized protein C11orf35 homolog (Lamin tail domain (LTD), homologous to intermediate filament containing protein)	43 50	VAPSY*SQSAK LY*TSTPMGCSVK	52.2 4.3
	C11orf65	Uncharacterized protein C11orf65 homolog	278	SLQSNIY*GDEAK	3.0
	Gm884	Novel protein Gm884 (Leucine-rich repeat)	749	TINPQIY*SQVK	4.6
Not-categorized					
	Als2cr11	Amyotrophic lateral sclerosis 2 (juvenile) chromosome region, candidate 11 (homologous to interaptin-like)	424	TTY*DIHHR	3.1

Category[a]	Symbol	Protein description	Position	Peptide sequence[b]	KO/WT[c]
			431	KY*EAISNEYGDK	1.5
	Theg	Testicular haploid expressed gene protein, Isoform 1	363	IY*ELATPK	3.2
	Maats1; Spata26	MAATS1 (AMY-1-associating protein expressed in testis 1 homolog)	179	Y*AIIPTK	3.1
	Ccdc136	Coiled-coil domain-containing protein 136	190	IRGDY*EMEIASLR	1.7
	Pex13	Peroxisomal membrane protein PEX13	194	YLY*RR	0.8
	Gtl3	UPF0468 protein C16orf80 homolog, isoform 1 (homologous to transcription factor II B, localized to cilium)	184	LY*LPVQNK	2.0

Peptide and protein FDR controlled to 1%.

[a] As determined by Gene Ontology (GO), NCBI BLASTp along with their conserved domains.

[b] *, phosphorylation; -, protein terminus.

[c] As determined by average CatSper1-KO/WT ratio normalized to protein expression. See Table S1 for full details.